Zhang *et al. EURASIP Journal on Advances in Signal Processing* (2016) 2016:99
DOI 10.1186/s13634-016-0391-6

EURASIP Journal on Advances in Signal Processing

RESEARCH Open Access

Array signal recovery algorithm for a single-RF-channel DBF array

Duo Zhang*, Wen Wu and Da Gang Fang

Abstract

An array signal recovery algorithm based on sparse signal reconstruction theory is proposed for a single-RF-channel digital beamforming (DBF) array. A single-RF-channel antenna array is a low-cost antenna array in which signals are obtained from all antenna elements by only one microwave digital receiver. The spatially parallel array signals are converted into time-sequence signals, which are then sampled by the system. The proposed algorithm uses these time-sequence samples to recover the original parallel array signals by exploiting the second-order sparse structure of the array signals. Additionally, an optimization method based on the artificial bee colony (ABC) algorithm is proposed to improve the reconstruction performance. Using the proposed algorithm, the motion compensation problem for the single-RF-channel DBF array can be solved effectively, and the angle and Doppler information for the target can be simultaneously estimated. The effectiveness of the proposed algorithms is demonstrated by the results of numerical simulations.

Keywords: Sparse reconstruction, Low-cost digital beamforming, Single-RF-channel, Artificial bee colony

1 Introduction

Digital beamforming (DBF) technology offers a significant improvement in performance over analog beamforming technology [1]. Many applications, including modern wireless communications, radar systems, surveillance, radio astronomy, and sonar, take advantage of this technology to gain benefits in terms of beam steering, improved signal-to-interference ratio (SIR), and interference rejection [2]. Recently, multi-input multi-output (MIMO) technology has attracted the attention of many researchers because it offers the ability to transmit multiple probe signals via transmit antennas, thereby providing additional diversity [3]. At the receiving end, DBF technology has been applied to sample combinations of reflected array signals from each element of an array to achieve different functions [4, 5]. Another research topic of interest is a type of flexible array called a frequency diverse array (FDA), which was proposed in [6, 7]. A small frequency increment is applied across all array elements to obtain a range-angle-dependent beam pattern. DBF technology has thus been used to enhance beamforming performance [8–10].

The DBF technique is based on the signals received at each antenna element. The set of such signals collected at a given instant of time constitutes a snapshot. The traditional way to obtain such snapshots is to connect each array element to an independent radio frequency (RF) receiver. Therefore, the number of receivers must be equal to the number of antenna elements, which usually causes the overall system to be complicated, bulky, and costly [11]. This problem becomes more serious in the case of large-scale arrays. Moreover, the channel uniformity, which significantly affects the performance of the system, should be carefully designed [12].

Various efforts have been made to reduce the hardware cost and design complexity of such systems. One feasible solution is to use a single-RF-channel structure in the antenna array. There are two main kinds of single-RF-channel structures, which use only one receiver channel and therefore are cost effective. The first is the switched antenna array (SAA), in which the connections of the antennas to the single receiving channel are periodically switched to sample the array signals. This structure was proposed in [13], and the corresponding array signal processing method has been discussed in [14–16]. However,

*Correspondence: duozhang@foxmail.com
Ministerial Key Laboratory of JGMT, School of Electronic Engineering and Optoelectronic Technology, Nanjing University of Science and Technology, 210094, Nanjing, China

although the number of low-noise amplifiers (LNAs) and mixers is reduced, the numbers of low-pass filters and analog-to-digital converters (ADCs) still must be proportional to the number of elements [17]. The second type of structure is the time sequence phase weighting (TSPW) antenna array [18, 19], in which the combined phase weighted array signals are sequentially sampled by a single RF-receiving channel. Each antenna element is followed by a 1-bit digitally controlled $0/\pi$ phase shifter. The weighted array signals are combined to form a single-channel output, and only one ADC is required to sample this output. In previous research, the base-band signal has typically been assumed to be time-invariant. This assumption is acceptable for most communication scenarios in which the sampling cycle is equal to the period of each data symbol [20, 21]. However, when the target has a relative radial velocity, the echo signal will contain a Doppler frequency, which causes the received signal to be time-varying. Therefore, a TSPW array cannot obtain the correct array signals in the case of movement. This is a key problem that must be addressed before the use of TSPW antenna arrays can become widespread.

A Doppler frequency compensation algorithm was proposed in [22] to solve this problem. By observing the targets for a certain length of time, the number of targets and the Doppler frequency of each target are estimated beforehand. This prior information is used to compensate the received single-channel-sampled signals to obtain the correct original signals. However, this algorithm requires pre-observation to estimate the number of targets and the Doppler frequencies, which obviously increases the total processing time. In [23], a time-reversal motion compensation algorithm was proposed to overcome this drawback. Without requiring prior information, this method allows the correct original array signals to be obtained through interpolation. However, this method requires the sampling frequency to be N times higher than that in a typical multichannel system. This requirement limits the application of this method for large-scale arrays.

In this paper, a sparse-reconstruction-based signal processing algorithm is proposed. It uses analog mixers and standard (high-rate) shift registers [24] to transform the spatially parallel array signals into time-sequence signals. This signal processing algorithm is quite different from that used in a TSPW array. A random sampling matrix is adopted in place of the Walsh-Hadamard matrix, which is used in TSPW arrays, to achieve the reduced-dimension transformation. The original spatially parallel array signals are recovered from the time-sequence sampled signals by exploiting the second-order sparse property of the array signals. No prior observation is required to obtain the number and Doppler information of the targets. The required sampling frequency is equal to that of a typical multichannel system. With the aid of the proposed algorithm, the direction of arrival (DOA) and the Doppler frequency of the target can be estimated simultaneously. Additionally, this paper also proposes a hardware-achievable measurement matrix optimization method based on the artificial bee colony (ABC) algorithm to improve the reconstruction performance in practical applications.

The remainder of this paper is organized as follows. In Section 2, the array structure and signal model are discussed. In Section 3, the sparse-reconstruction-based signal processing algorithm is proposed. To improve the reconstruction performance, a method for optimizing the measurement matrix, which is based on the artificial bee colony (ABC) algorithm, is proposed in Section 4. The simulation results are provided in Section 5 to demonstrate the effectiveness of the proposed algorithm. Conclusions are given in Section 6.

2 The system model

2.1 Single-RF-channel DBF array

The structure of the single-RF-channel DBF array is shown in Fig. 1. It is similar to that of a TSPW array. The difference is that the 1-bit digitally controlled phase shifters are replaced with analog mixers and standard (high-rate) shift registers to increase the bandwidth of the system [24]. To highlight the signal processing flow, the diagram eliminates several components that may be used in a practical system, such as band-pass filters, low-pass filters, IF amplifiers, quadrature detectors, and so on.

2.2 Signal model

To simplify the analysis, this paper adopts the following assumptions. (1) The echo signal is assumed to be the far-field narrowband signal. (2) The target is moving with a constant relative velocity within one transformation period T_{single}, where T_{single} = 1/PRF. In other words, the Doppler frequency f_d exhibits no significant change during one T_{single}. 3). The direction of arrival (DOA) of the target does not change within one T_{single}.

The signal received by the nth antenna can be considered as being modulated by the rectangular pulse $rect$(t) and can be written as [25]

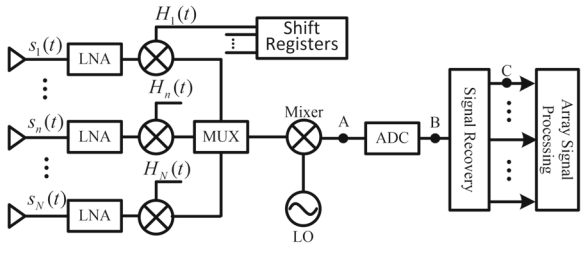

Fig. 1 The structure diagrams of single-RF-channel DBF array

$$s_n(t) = \sum_{m=-\infty}^{m=\infty} rect\left(t - mT_{single}\right) Re\left[\sum_{k=1}^{K} z_k(t) e^{j\Delta\phi_n} e^{j2\pi f_c t}\right] \tag{1}$$

where $n = 1, 2, \ldots, N$, f_c is the carry frequency, and $j^2 = -1$. $z_k(t) = e^{j4\pi(R_k - v_k t)/\lambda_c}$ is the base-band echo signal of the kth target, where R_k and v_k are the initial range and the velocity, respectively, of the kth target. $\Delta\phi_{k,n} = 2\pi\ (n-1)\ d\sin(\theta_k)/\lambda_c$ is the spatial phase difference between the nth element and the first element that is produced by the echo of the kth target, where the element spacing is d and θ_k is the angle of kth target. Let

$$x_n(t) = \sum_{k=1}^{K} z_k(t) e^{j\Delta\phi_{k,n}} = \tilde{z}(t) e^{j\Delta\tilde{\phi}_n} \tag{2}$$

denote the base-band signal received by the nth element. The frequency of $x_n(t)$ induced by the kth target is $f_{d,k} = 2v_k/\lambda_c$, where λ_c is the wavelength. Let $Q(t) = \sum_{m=-\infty}^{m=\infty} rect\left(t - mT_{single}\right)$. Equation (1) then can be rewritten as

$$s_n(t) = Q(t) Re\left[x_n(t) e^{j2\pi f_c t}\right] \qquad n = 1, \ldots, N \tag{3}$$

Let the weighting value assigned to the nth phase shift at time instant t be denoted by $H_n(t)$. The N-dimensional array signal after weighting, combining, and down-converting, is converted into a one-dimensional single-channel signal (point a in Fig. 1). In practice, the signal at point A is a complex signal and is usually represented by both in-phase (I) and quadrature (Q) paths. However, Fig. 1 shows only a single path for simplicity. The signal can be expressed as

$$S_A(t) = Q(t) \sum_{n=1}^{N} \{G_n H_n(t)[x_n(t) + \varepsilon_n(t)]\} \tag{4}$$

where G_n is the gain of the nth low noise amplifier (LNA) and $\varepsilon_n(t)$ is the receiver noise of the nth element.

Within the duration of each pulse, the signal $S_A(t)$ can be sampled many times by only one analog to digital converter (ADC) in accordance with the sampling frequency. The average data can be used as the final weighted result for a signal pulse. For minimum-sampling-rate operation, the sampling rate of the ADC is equal to the PRF and only one sample is taken at the end of each pulse. The signal at point B is called the *single-channel-sampled* signal and can be expressed as

$$S_B(mT_{single}) = \sum_{n=1}^{N} \left\{G_n H_n(mT_{single}) \left[x_n(mT_{single}) + \varepsilon_n(mT_{single})\right]\right\} \tag{5}$$

After M pulses, the signal $S_B(mT_{single})$ has been multiplied by $H_n(mT_{single})$, $m = 1, \ldots, M$. It contains all of the information of the target and can be used to recover the original signals. The signal at point C represents the recovered spatially parallel signal for the ith single-channel-sampling period.

When the target is static, the base-band signal received at the nth element $x_n(t)$ can be regarded as a time-constant signal in one T_{single}. It can be denoted as $x_n(1) \approx \cdots \approx x_n(M) = \tilde{x}_n$. When the target is moving, the base-band signal $x_n(t)$ is a time-varying signal. The amplitude and phase may vary significantly in one T_{single}. A Doppler phase difference $\Delta\tilde{\varphi}_{f_d}$ is added to the adjacent single-channel sampled signals. The first sampling performed in one T_{single} is taken as the reference point. The signals at other sampling times in one T_{single} can then be written as

$$x_n(m) = x_n(1) e^{j(m-1)\Delta\tilde{\varphi}_{f_d}} = \tilde{z}(1) e^{j(m-1)\Delta\tilde{\varphi}_{f_d}} e^{j\Delta\tilde{\phi}_n} \tag{6}$$

It can be seen that the signal is disturbed by both the Doppler phase difference $\Delta\tilde{\varphi}_{f_d}$ and the spatial phase difference $\Delta\tilde{\phi}_n$. If the matrix inversion algorithm proposed in [19] was still to be used to obtain the original signals, then the recovered signal $S_{C,n}(iT_{single})$ would contain incorrect target information and could not be used for further signal processing.

3 Sparse-reconstruction-based signal processing

3.1 Time-sequence sampling model

Before sparse reconstruction theory can be applied, the time-sequence sampling model should first be established. Equation (5) can be rewritten in matrix form as

$$S_B(m) = < \mathbf{G} \odot \mathbf{\Phi}(m), \mathbf{x}(m) > + \sigma(m) \tag{7}$$

where $\mathbf{G} = [G_1, \cdots, G_N]^T$; $\mathbf{\Phi}(m) = [H_1(m), \cdots, H_N(m)]^T$; $\mathbf{x}(m) = [x_1(m), \cdots, x_N(m)]^T$; $\odot$ and $<,>$ denote the Hadamard product and the inner product, respectively; and $\sigma(m)$ is the receiver noise. The weighting vector $\mathbf{\Phi}(m)$ is produced by the analog mixers and shift registers shown in Fig. 1, and the value of each element of $\mathbf{\Phi}(m)$ is 1 or -1. Thus, the vector $\mathbf{\Phi}(m)$ can be designed as a Bernoulli random vector, which also consists of values of ± 1 and has a low coherence with any fixed basis.

After M pulses, the single-channel-sampled signals can be grouped into a vector $\mathbf{Y}_{1:M}$ as follows:

$$\mathbf{Y}_{1:M} = \begin{bmatrix} S_B(1) \\ \vdots \\ S_B(M) \end{bmatrix} = \begin{bmatrix} < \mathbf{G} \odot \mathbf{\Phi}(1), \mathbf{x}(1) > \\ \vdots \\ < \mathbf{G} \odot \mathbf{\Phi}(M), \mathbf{x}(M) > \end{bmatrix} + \sigma \tag{8}$$

where $\sigma = [\sigma(1), \cdots, \sigma(M)]^T$ is the M-dimensional noise vector. Equation (8) is a natural mathematical

description of the processing of the single-channel-sampled signals. However, it is not in a standard matrix operation form and cannot be directly solved. An equivalent standard matrix form of (8) is

$$\begin{aligned}\mathbf{Y}_{1:M} &= \bar{\mathbf{\Phi}}\mathbf{X} \\ &= \begin{bmatrix} \mathbf{G}\odot\mathbf{\Phi}(1) & \mathbf{0} & \dots & \mathbf{0} \\ \mathbf{0} & \mathbf{G}\odot\mathbf{\Phi}(2) & \dots & \mathbf{0} \\ \vdots & \vdots & & \vdots \\ \mathbf{0} & \mathbf{0} & \dots & \mathbf{G}\odot\mathbf{\Phi}(M) \end{bmatrix} \begin{bmatrix} \mathbf{x}(1) \\ \mathbf{x}(2) \\ \vdots \\ \mathbf{x}(M) \end{bmatrix} + \sigma \end{aligned} \tag{9}$$

where $\bar{\mathbf{\Phi}}$ is the equivalent measurement matrix and $\mathbf{0}$ is a $1 \times N$ zero vector.

The (NM)-dimensional vector signal $\mathbf{X} = [\mathbf{x}^T(1), \cdots, \mathbf{x}^T(M)]^T$ contains the same information as that contained in the multi-snapshot array signal $\tilde{\mathbf{X}} = [\mathbf{x}(1), \cdots, \mathbf{x}(m)]$, which is the $N \times M$-dimensional matrix obtained by a normal multichannel DBF array. However, there are certain differences between these two signals. The signal $\tilde{\mathbf{X}}$ has a parallel structure and is obtained by directly sampling the signals from each array element with multiple receivers. It is known immediately after sampling. By contrast, the signal $\mathbf{X}$ has a sequential structure and cannot be obtained directly after sampling. It is wrapped in the *single-channel-sampled* vector $\mathbf{Y}_{1:M}$ which consists of the real signals sampled in the single-channel DBF system.

3.2 The first-order sparse expression for the array signal

The signal $\mathbf{X}$ can be recovered using sparse signal reconstruction theory, if and only if the signal is sparse or compressible [26–28]. According to the spatial sparsity feature of array signals [29–31], an array signal at time instant m is spatially sparse. The desired angular region can be decomposed into $P \geq N$ segments. Let $\theta = [\tilde{\theta}_1, \cdots, \tilde{\theta}_P]$, where $\tilde{\theta}_p$ denotes the central direction of the pth segment. The N-dimensional base-band array signal at time instant m can be expressed as

$$\boldsymbol{x}(m) = \mathbf{\Psi}\boldsymbol{\xi}(m) \tag{10}$$

where $\boldsymbol{\xi}(m)$ is a P-dimensional spatially sparse projection vector. Because the vector $\boldsymbol{\xi}(m)$ is sparse [30], it has only $K \ll N \leq P$ nonzero entries. The matrix $\mathbf{\Psi} = [\mathbf{a}\left(\tilde{\theta}_1\right), \cdots, \mathbf{a}(\tilde{\theta}_P)]$ is a sparse transformation matrix which based on the steering vector. The steering vector [32] is defined as $\mathbf{a}\left(\tilde{\theta}_p\right) = \left[1, \cdots, \mathrm{e}^{\mathrm{j}2\pi(N-1)d\sin\left(\tilde{\theta}_p\right)/\lambda_c}\right]^T$. Using Eq. (10), the array signal $\mathbf{X}$ can be expressed as

$$\mathbf{X} = \begin{bmatrix} \mathbf{\Psi} & \mathbf{0} & \cdots & \mathbf{0} \\ \mathbf{0} & \mathbf{\Psi} & \cdots & \mathbf{0} \\ \vdots & \vdots & & \vdots \\ \mathbf{0} & \mathbf{0} & \cdots & \mathbf{\Psi} \end{bmatrix} \begin{bmatrix} \xi(1) \\ \xi(2) \\ \vdots \\ \xi(M) \end{bmatrix} \tag{11}$$

Because Eq. (11) transforms the array signal only in spatial domain, it can be regarded as the first-order sparse expression of the array signal. However, the signal $\mathbf{X}$ contains M snapshots, and the time information has been added into the signal. The sparse projection vector $\tilde{\boldsymbol{\xi}} = [\boldsymbol{\xi}^T(1), \cdots, \boldsymbol{\xi}^T(M)]^T$ will have $K \times M$ nonzero entries, which causes (11) to be an imperfect sparse expression. The signal $\mathbf{X}$ should be written in a sparser form to ensure a better performance before applying sparse reconstruction theory to recover it.

3.3 The second-order sparse expression for the array signal

The time information of an array signal is associated with the Doppler frequency of the target. Because the number of targets is usually limited, the Doppler frequencies of the targets are also sparse with respect to the entire Doppler frequency spectrum. In radar signal processing theory, the Fourier transform is a common tool for obtaining Doppler information. Let the Fourier transform matrix be denoted by $\mathbf{F} \in \mathbb{C}^{\mathbf{M}\times\mathbf{M}}$. Then, the first-order sparse projection vector $\tilde{\boldsymbol{\xi}} = \left[\boldsymbol{\xi}^T(1), \cdots, \boldsymbol{\xi}^T(M)\right]^T$ can be written in second-order projection form as

$$\tilde{\boldsymbol{\xi}} = \left[\left(\mathbf{F}^{-1}\right)^T \otimes \mathbf{I}_P\right]\boldsymbol{\chi} \tag{12}$$

where $\mathbf{F}^{-1}$ is the inverse Fourier transform matrix, $\mathbf{I}_P$ is a $P \times P$ unit matrix, $\boldsymbol{\chi}$ is a K-sparse (PM)-dimensional vector, and $\otimes$ is the right Kronecker product of two matrices. A schematic diagram of the transformation of the first-order projection into the second-order projection is shown in Fig. 2.

To illustrate the advantages of the second-order sparse property of the array signal, Fig. 3 compares the sparsity of the first-order projection vector $\tilde{\boldsymbol{\xi}}$ with that of the second-order projection vector $\boldsymbol{\chi}$. Six spatial signals are assumed to be arriving at the front of the system from six different directions and at different velocities. The number of angles is P = 180, and M = 200. The signal-to-noise ratio (SNR) is equal to 10 dB. The SNR is defined as the ratio of the signal power to the observed noise power. The first 8000 entries of these two projection vectors with descending indices are shown. It can be seen that the number of nonzero entries of the vector $\tilde{\boldsymbol{\xi}}$ is much greater than that of the vector $\boldsymbol{\chi}$. The l_0-norm of the first-order vector, which is also the number of nonzero entries, is 6557, whereas that of the second-order vector is 448. Thus, by using the second-order sparse projection vector, the number of nonzero entries is reduced by approximately 93.2 %, demonstrating that the second-order sparse projection of the array signal is more suitable than the first-order projection for recovering the array signal $\mathbf{X}$.

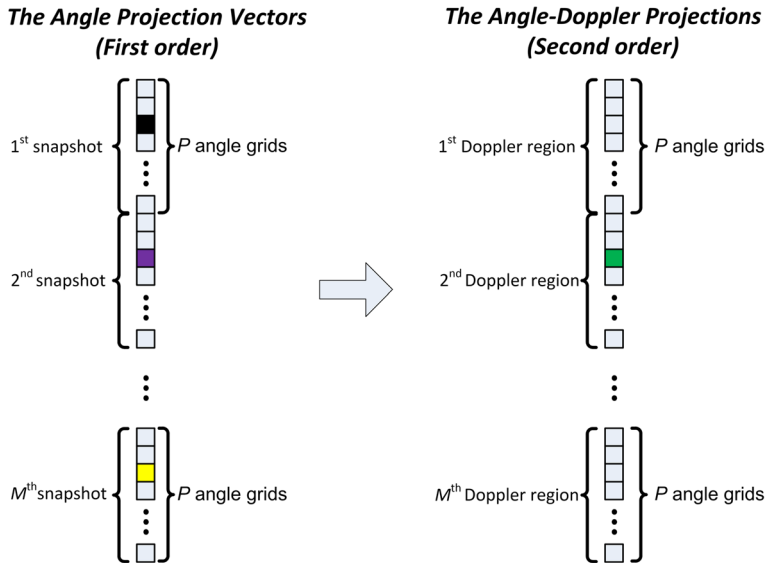

Fig. 2 The transforming schematic diagram

The substitution of (12) into (11) and the application of the properties of the Kronecker product together yield the following second-order sparse expression for the array signal:

$$\mathbf{X} = \left[\left(\mathbf{F}^{-1}\right)^{T} \otimes \mathbf{\Psi}\right] \boldsymbol{\chi} \tag{13}$$

3.4 Sparse reconstruction

By utilizing the second-order sparse expression (13) and the single-channel sampling model (9), the single-channel sampling vector can be rewritten as

$$\mathbf{Y}_{1:M} = \bar{\mathbf{\Phi}}\bar{\mathbf{\Psi}}\boldsymbol{\chi} + \boldsymbol{\sigma} \tag{14}$$

where $\bar{\mathbf{\Psi}} = \left[\left(\mathbf{F}^{-1}\right)^{T} \otimes \mathbf{\Psi}\right]$ is the second-order joint angle-Doppler sparse transform matrix for the array signal.

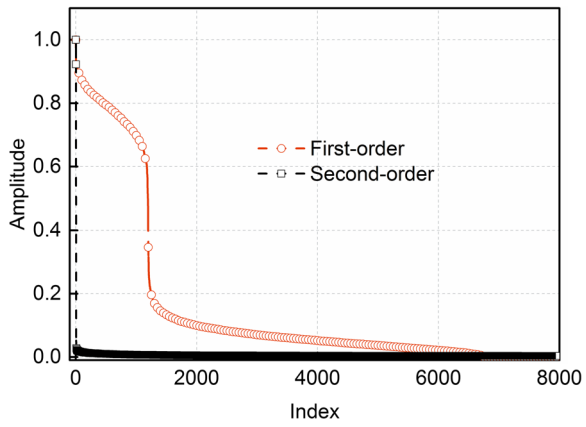

Fig. 3 The first-order and second-order sparse projection vectors of array signal

Theoretical studies [33] show that the equivalent sensing matrix $\mathbf{D} = \bar{\mathbf{\Phi}}\bar{\mathbf{\Psi}}$ will satisfy the condition of the restricted isometry property (RIP) with high probability if the number of single-channel measurements M in one sampling cycle T_{single} satisfies

$$M \geq C_0 K \log(N/K) \tag{15}$$

where C_0 is a positive constant. Notably, increasing M can improve the Doppler frequency resolution at the cost of significantly extending the processing time. There is therefore a trade-off between the performance and the processing time cost in practical applications.

Equation (14) is a classical Lasso problem and can be solved by solving the following equation:

$$\bar{\boldsymbol{\chi}} = \arg\min_{\boldsymbol{\chi}} \frac{1}{2} \left\| \bar{\mathbf{\Phi}}\bar{\mathbf{\Psi}}\boldsymbol{\chi} - \mathbf{Y}_{1:M} \right\|_2^2 + \eta \|\boldsymbol{\chi}\|_1 \tag{16}$$

where $\eta > 0$ is the regularization parameter, which corresponds to the noise power, and $\|\cdot\|_1$ denotes the l_1-norm, which is equal to the sum of the absolute values of the vector entries. The parameter η controls the trade-off between the sparsity approximation and the least square error of the recovered signal [34]. The parameter selection method has been comprehensively studied in [35], and we therefore omit such a discussion in this paper.

The recovered second-order projection vector $\bar{\boldsymbol{\chi}}$ contains the angle information and the Doppler frequencies of the targets. After the vector has been obtained, the original array signals from all M samplings can be recovered as follows:

$$\hat{X} = \mathbf{\Psi} unvec_{M,P}(\bar{\boldsymbol{\chi}})\mathbf{F}^{-1} \tag{17}$$

where $unvec_{M,P}(\cdot)$ is the inverse vectorization function such that $unvec_{M,P}(\bar{\boldsymbol{\chi}})$ is an $M \times P$ matrix that enables the conversion from the $MP \times 1$ vector $\bar{\boldsymbol{\chi}}$.

4 Optimization

4.1 Optimization of the measurement matrix

Because analog mixers and shift registers can easily be realized in practical applications, they are used in the single-channel DBF array to measure the array signals. The shift registers provide only two phase-weighting states. Therefore, the measurement matrix $\boldsymbol{\Phi}$ consists of values of ± 1.

The measurement matrix can be optimized to achieve better reconstruction performance [36–39]. However, the existing algorithms generally ignore the practical problem that arises when the values of the optimal measurement matrix elements are too precise to be achieved by the hardware. In other words, the hardware-based measurement matrix generally cannot provide the measurement values that are produced by such optimization algorithms. For example, the digital micromirror device (DMD) in a single-pixel camera [40] cannot provide reflection directions other than $\pm 10°$. The recovery algorithm based on the single-RF-channel DBF array also faces the same problem. Thus, to improve the reconstruction performance, an optimization algorithm is proposed that can produce hardware-realizable measurement values.

Let $\tilde{\mathbf{D}}$ denote the column normalized form of the equivalent sensing matrix $\mathbf{D}$. The mutual-coherence of $\mathbf{D}$ is defined as

$$\mu(\mathbf{D}) = \max[\, triu(\mathbf{L})] \tag{18}$$

where $\mathbf{L} = \tilde{\mathbf{D}}^H \tilde{\mathbf{D}}$ is the so-called Gram matrix and $triu(\cdot)$ is a function such that $triu(\mathbf{L})$ extracts the upper triangular entries from the off-diagonal part of the matrix $\mathbf{L}$. To achieve high-reconstruction performance, the value of (18) should be designed to be as small as possible [41]. From section 3.4, we know that $\bar{\boldsymbol{\Psi}}$ is a fixed matrix associated with the detection requirements; therefore, we can optimize only $\bar{\boldsymbol{\Phi}}$ to reduce $\mu(\mathbf{D})$.

Based on the fact that the hardware can provide only two weighting values of ± 1, all possible observations form the feasible solution set $\boldsymbol{\Omega}$. The optimal observation matrix $\boldsymbol{\Phi}_{opt}$ that minimizes $\mu(\mathbf{D})$ must be included in this set. For a single-RF-channel system with N elements and M observations, the number of feasible solutions in $\boldsymbol{\Omega}$ is 2^{NM}. Directly finding an optimal solution from within this enormous feasible set is certainly an NP-hard problem.

The Artificial Bee Colony (ABC) algorithm is a swarm-based meta-heuristic algorithm [42] that is suitable for solving this optimization problem. It finds the optimal solution by simulating the behavior of bees. The model used in the ABC algorithm consists of three essential components: food sources, employed foraging bees, and unemployed foraging bees. The artificial bees can move toward better solutions by means of a neighbor search mechanism, while abandoning poor solutions. When using the ABC algorithm, a rough objective function can be selected as described below:

$$\begin{aligned} \boldsymbol{\Phi}_{opt} &= \min_{\bar{\boldsymbol{\Phi}}} \mu(\mathbf{D}) \\ s.t. \bar{\boldsymbol{\Phi}} &\subseteq \Omega \\ \mathbf{D} &= \bar{\boldsymbol{\Phi}} \bar{\boldsymbol{\Psi}} \end{aligned} \tag{19}$$

The steps of the ABC algorithm for optimizing the measurement matrix for the recovery algorithm are as follows.

1) The control parameters are initialized, and the initial food sources are prepared. Each food source is a feasible matrix from the collection Ω. The Bernoulli random matrix can be used for initialization.
2) The employed bees search for new food sources within the neighborhood of the current food source. The strategy for determining neighboring food sources is described as follows:
   - **(a)** A zero entry of the matrix $\bar{\Phi}_m - \bar{\Phi}_k$ is randomly selected, where $\bar{\Phi}_m$ is the current food source and $\bar{\Phi}_k$ is the randomly selected neighboring food source.
   - **(b)** The element value of $\bar{\Phi}_m$ is reversed at the position selected in a).
   - **(c)** The new food source is used to calculate the fitness value by applying the function described in [42]
3) The unemployed bees then work to find the best solutions.
4) If the maximum number of cycles has been reached, then the algorithm terminates and outputs the optimal solution. Otherwise, the process is repeated from step 2.

4.2 Optimization of the computational complexity

The numbers of angle grids P and single-channel samplings M influence the angular and velocity resolutions, respectively, of the recovery algorithm. The values of these two parameters can be increased to improve the recovery performance. However, this will significantly increase the computational complexity. To reduce the computational complexity for practical applications, a coarse grid can be used first to find the approximate source information. Then, the neighboring regions of the targets can be searched again, using a finer grid. The accurate sparse projection vector is thus obtained by using a fine grid in a few small regions.

In practice, when searching in these small regions, the processing time can be shortened by using multiple Digital Signal Processors (DSPs) with a parallel structure. The search region can be separated into several segments according to the angle and Doppler information shown in Fig. 2. Based on the detection results obtained using the coarse grid, the corresponding segments can be extracted and assigned to multiple processors to search for more accurate results with finer grids.

Table 1 shows the CPU processing times achieved while processing data of different scales. The experiments were performed on a platform with a Core i7-4710MQ CPU 2.50GHz, 8 GB of RAM, and the Windows 7 operating system. The computations of the method could be performed in a reasonable time on this platform. Because the processing time for the fast Fourier transform (FFT) can be greatly reduced by embedding the transform in a Field-Programmable Gate Array (FPGA), the processing time of this method can thus be shortened even further.

The processing time of the proposed algorithm includes two primary components. The first is the time consumption of the single-channel sampling procedure. This procedure has the same complexity as that for a typical multichannel DBF array, which is O(M). The second component is the time consumption of the sparse reconstruction procedure. The computational complexity of this procedure primarily depends on the chosen recovery algorithm. For example, the computational complexity of the recovery algorithm used in this paper is O($(MP)^3$) [43]. However, this recovery algorithm could be replaced with a faster one. For example, the Orthogonal Matching Pursuit (OMP) algorithm could be adopted, in which case the computational complexity would be O(KM^2P).

5 Simulation results

In this section, several numerical simulations are presented to evaluate the proposed algorithms. First, the original spatially parallel signals are recovered using the proposed algorithm, and the results are compared with those that are obtained directly by a typical multichannel DBF array in a moving scenario. Second, the ability of the proposed algorithm to simultaneously estimate the angle and Doppler information of the targets is evaluated by means of a classical parameter estimation problem.

Table 1 The CPU processing time

W	P	Angle resolution (degree)	Velocity resolution (m/s)	CPU time (s)	CPU time of parallel structure (s)
100	30	3	30	2.24	0.96
100	90	1	30	4.19	1.18
200	180	0.5	15	66.47	11.87
300	180	0.5	10	147.71	24.80

Finally, a simulation is presented to demonstrate the performance improvement achieved using the proposed measurement matrix optimization method.

A linear X-band antenna array with $N = 64$ elements is used. The spacing of the adjacent elements is 0.5λ, and the center frequency is 10 GHz. The PRF is 200 kHz, the number of single-channel samples is $M = 200$, and the number of angle grids is $P = 180$. The receiver noise is assumed to be zero-mean Gaussian white noise.

5.1 Evaluation of the signal reconstruction

In this section, the array signals received at each element that are recovered by the proposed algorithm are compared with those directly obtained by a typical multichannel DBF array. To demonstrate the effectiveness of the proposed algorithm, the processing results obtained using the algorithm presented in [44] are also proposed. Assume that there are three targets in front of the antenna. The azimuth angles are 10°, −20°, and 45°. First, the signals that are received when these targets are static are given in Fig. 4a. It can be seen that all systems obtain the same array signals, which demonstrates that they exhibit the same beamforming performance in static scenario. Second, we consider a scenario in which the velocities of these targets are 135, 240, and 45 m/s, respectively. The recovery results for this scenario are shown in Fig. 4b. It can be seen that the reconstruction algorithm used in [44] cannot obtain the correct original signals in the moving scenario, whereas the proposed algorithm can do so.

It is worth mentioning that the proposed algorithm does not require additional time to be spent in obtaining the number of targets and their Doppler frequencies as prior information and that the required PRF is equal to that for the multichannel system. Table 2 compares the requirements of the proposed algorithm with those of two other algorithms proposed in [22] and [23].

Figure 5 shows the average recovery errors as a function of the SNR. For comparison, the results produced by the algorithms proposed in [22] and [23] are also represented. The number of targets is 1, 2, and 3 respectively. Different directions and different Doppler frequencies are randomly selected in each trial. Monte Carlo simulations were performed 500 times to verify the average recovery error between the true and reconstructed signals. The recovery error is defined as

$$\mathrm{MSE} = 20\log_{10}E\left(\frac{\left\|\hat{\mathbf{X}}-\mathbf{X}\right\|_2^2}{\|\mathbf{X}\|_2^2}\right) \tag{20}$$

The performance of the algorithm proposed in [22] is associated with the frequency estimation errors. When the frequencies of two targets are close to each other,

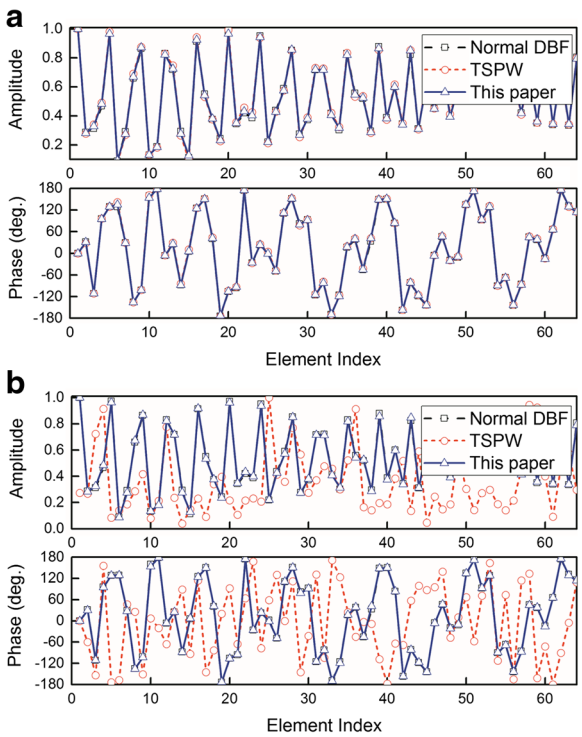

Fig. 4 The amplitude and phase signals received by each antenna element in the **a** static and **b** moving scenarios, respectively

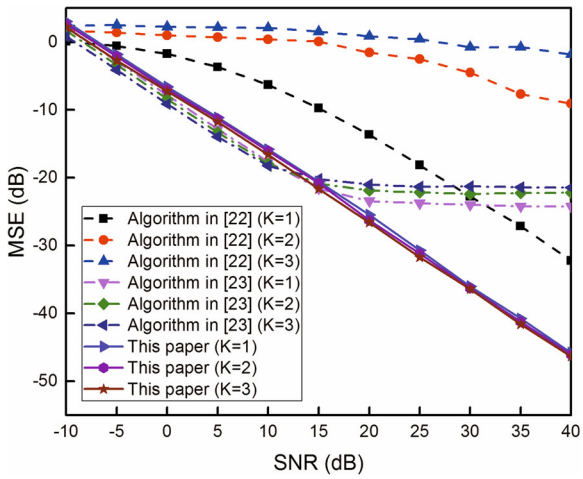

Fig. 5 The average recovery errors as a function of SNR

it becomes difficult to distinguish them with the normal methods. This may cause a serious decline in recovery performance. The performance of the algorithm proposed in [23] is associated with the number of samples. More samples will obtain a higher reconstruction accuracy. However, it will spend much more time in sampling and computing. In this simulation, the number of samples is 1024, which is four times as much as that used in the proposed method. It can be seen from Fig. 5 that the recovery error of the proposed method is less than −10 dB when the SNR is greater than 0 dB. However, in the low-SNR scenario, the algorithm fails to function properly.

5.2 Parameter estimation

The proposed algorithm can simultaneously obtain the angle and Doppler information for the targets. A parameter estimation problem in classical array signal processing is considered to evaluate this capability. Assume that there are three targets in front of the system. The azimuth angles are 3°, 4.5°, and −5°, and the velocities are 30, 60, and −75 m/s, respectively. The Doppler frequencies are 2, 4, and −5 kHz, respectively. A positive frequency is defined as one for which the target is moving toward the system. The SNR is 10 dB. Figure 6 shows the estimated results for the two-dimensional angle-Doppler spectrum.

It can be seen that the angle and Doppler information of the targets are estimated correctly. Moreover, it can be seen from the estimated results for targets A and B that the sources can be resolved even when the angle of separation between them is less than the classical Rayleigh resolution limit. This finding indicates that the algorithm has the capability of angular super-resolution.

Table 2 The comparison of requirements

	Normal DBF radar	Method in [22]	Method in [23]	This paper
Priori information	No need	Need	No need	No need
Samping frequency	PRF	PRF	N × PRF	PRF
Number of receiving channels	N	1	1	1

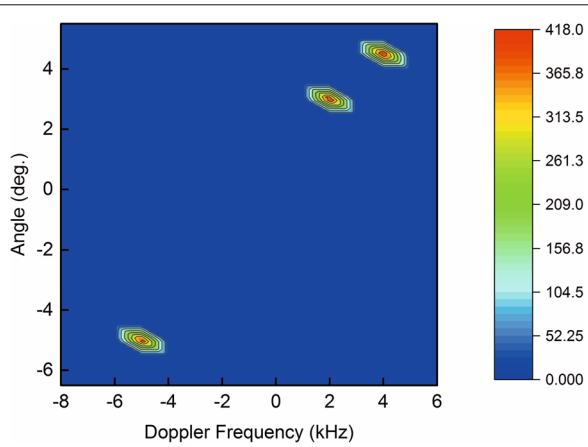

Fig. 6 The angel-Doppler spectrum estimated by the proposed algorithm

5.3 Optimization of the measurement matrix

In this subsection, the measurement matrix optimization method is evaluated. For these calculations, the parameters of the ABC algorithm were set as follows: the number of employed and unemployed bees is 40, the number of food sources is 20, and the number of cycles for foraging is 3000.

The histograms in Fig. 7 show the distribution of the absolute values of $\mu(\mathbf{D})$. For comparison, 500 random Bernoulli measurement matrices were generated in 500 trials. The worst and best results, which have the largest and smallest values of $\mu(\mathbf{D})$, respectively, among the 500 random matrices, are shown in Fig. 7a, b, respectively. It can be seen that the mutual-coherence of the best result is reduced by approximately 13 % with respect to that of the worst. However, when the optimization method is used, the mutual-coherence is further reduced by 10 % compared with that of the best result.

5.4 Simulations of the weighting circuit error

The weighting circuit that is used in a practical application is subject to gain and phase shift errors. Because these errors generate a non-orthogonal Walsh-Hadamard measurement matrix, these errors can result in completely incorrect recovered array signals.

However, the measurement matrix used in the proposed algorithm is required only to satisfy a certain probability distribution. The requirements on the absolute gain and phase shift values can be relaxed. Thus, the influence of the imperfections of the device can be greatly reduced.

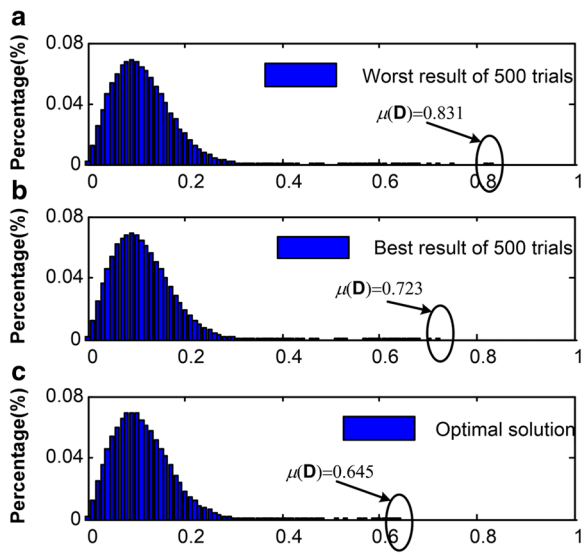

Fig. 7 The histograms of absolute entries of $\mu(\mathbf{D})$ before and after optimization. **a** and **b** are the worst and best result of 500 trials, respectively. **c** is the optimal result

Figure 8 presents a reconstruction result obtained when the weighting circuit is not ideal. One static target with an incidence angle of 3° is assumed to be present in front of the array. The amplitude and phase shift errors are within 15 % and 30°, respectively. The results presented in Fig. 8 indicate that the proposed algorithm is robust to amplitude and phase errors in the weighting circuit. In addition, a correction technique is also available when needed.

6 Conclusions

Array signal processing algorithms based on sparse signal reconstruction are proposed for a low-cost single-channel DBF array. The second-order sparse property of the array signals is used to decouple the angle and velocity information and to obtain the correct original parallel array signals from the weighted time-sequence signals. The DOA and Doppler information of the targets can be simultaneously

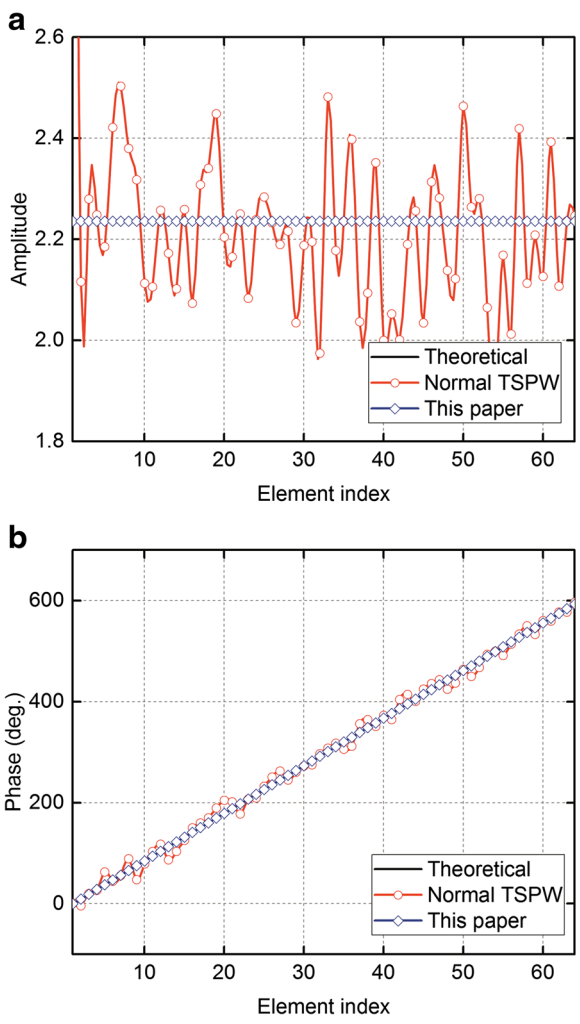

Fig. 8 The reconstruction results when the weighting circuit is not ideal. **a** and **b** are the amplitude and phase, respectively

estimated using this low-cost scheme, which uses a low-cost, high-efficiency receiver array in place of the traditional design. The proposed approach can be adopted in several expensive and complicated array systems, such as FDAs and MIMO systems, to reduce their total cost.

Competing interests
The authors declare that they have no competing interests.

Received: 1 May 2016 Accepted: 25 August 2016
Published online: 14 September 2016

References

1. P Barton, Digital beam forming for radar. IEE Proc. F (Commun. Radar Signal Process.) **127**(4), 266–277 (1980)
2. S Bellofiore, CA Balanis, J Foutz, AS Spanias, Smart-antenna systems for mobile communication networks. part 1. overview and antenna design. IEEE Antennas Propag. Mag. **44**(3), 145–154 (2002)
3. J Li, P Stoica, Mimo radar with colocated antennas. IEEE Signal Process. Mag. **24**(5), 106–114 (2007)
4. F Belfiori, L Anitori, W van Rossum, M Otten, P Hoogeboom, in *2011 European Radar Conference (EuRAD)*. Digital beam forming and compressive sensing based doa estimation in mimo arrays, (Manchester, 2011), pp. 285–288
5. C Xiang, D-Z Feng, H Lv, J He, Y Cao, Robust adaptive beamforming for mimo radar. Signal Process. **90**(12), 3185–3196 (2010)
6. P Antonik, MC Wicks, HD Griffiths, CJ Baker, in *2006 IEEE Conference on Radar*. Frequency diverse array radars, (Verona, NY, 2006), p. 3
7. K Gao, H Chen, H Shao, J Cai, W-Q Wang, Impacts of frequency increment errors on frequency diverse array beampattern. EURASIP J. Adv. Signal Process. **2015**(1), 1–12 (2015)
8. AM Jones, BD Rigling, in *2012 International Waveform Diversity & Design Conference (WDD)*. Frequency diverse array radar receiver architectures, (Kauai, HI, 2012), pp. 211–217
9. J Xu, G Liao, S Zhu, in *2014 XXXIth URSI General Assembly and Scientific Symposium (URSI GASS)*. Receive beamforming of frequency diverse array radar systems, (Beijing, CHN, 2014), pp. 1–4
10. WQ Wang, Phased-mimo radar with frequency diversity for range-dependent beamforming. IEEE Sensors J. **13**(4), 1320–1328 (2013)
11. JD Fredrick, W Yuanxun, T Itoh, Smart antennas based on spatial multiplexing of local elements (smile) for mutual coupling reduction. IEEE Trans. Antennas Propag. **52**(1), 106–114 (2004)
12. ML Morris, MA Jensen, Impact of receive amplifier signal coupling on mimo system performance. IEEE Trans. Vehic. Technol. **54**(5), 1678–1683 (2005)
13. JD Fredrick, W Yuanxun, T Itoh, A smart antenna receiver array using a single rf channel and digital beamforming. IEEE Trans. Microwave Theory Tech. **50**(12), 3052–3058 (2002)
14. L Moon-Sik, V Katkovnik, K Yong-Hoon, System modeling and signal processing for a switch antenna array radar. IEEE Trans. Signal Process. **52**(6), 1513–1523 (2004)
15. H Chenxi, L Yimin, M Huadong, W Xiqin, Randomized switched antenna array fmcw radar for automotive applications. IEEE Trans. Vehic. Technol. **63**(8), 3624–3641 (2014)
16. S Henault, BR Jackson, YMM Antar, Compensation of time-division multiplexing distortion in switched antenna arrays with a single rf front-end and digitizer. IEEE Trans. Antennas Propag. **61**(8), 4383–4388 (2013)
17. G Krishnamurthy, KG Gard, Time division multiplexing front-ends for multiantenna integrated wireless receivers. IEEE Trans. Circuits Systems I: Regular Papers. **57**(6), 1231–1243 (2010)
18. DG Fang, S JinTao, W Yin, W-X Sheng, Realization of radar cross-range resolution by array phase weighting. Chin. J. Radio Sci. **10**(1), 1–3 (1995)
19. J Zhang, W Wu, D-G Fang, Single rf channel digital beamforming multibeam antenna array based on time sequence phase weighting. IEEE Antennas Wireless Propag. Lett. **10**, 514–516 (2011)
20. EA Alwan, SB Venkatakrishnan, AA Akhiyat, W Khalil, JL Volakis, Code optimization for a code-modulated rf front end. IEEE Access. **3**, 260–273 (2015)
21. A Jahanian, F Tzeng, P Heydari, Code-modulated path-sharing multi-antenna receivers: theory and analysis. IEEE Trans. Wireless Commun. **8**(5), 2193–2201 (2009)
22. W-X Sheng, D-G Fang, Angular superresolution for phased antenna array by phase weighting. IEEE Trans. Aerospace Electron. Syst. **37**(4), 1450–1814 (2001)
23. D Zhang, W Wu, DG Fang, in *2015 Asia-Pacific Microwave Conference (APMC)*. A novel motion compensation method for single rf channel digital beamforming array, (Nanjing, CHN, 2015), pp. 1–3
24. M Mishali, YC Eldar, From theory to practice: Sub-nyquist sampling of sparse wideband analog signals. IEEE J. Selected Topics Signal Process. **4**(2), 375–391 (2010)
25. YH Quan, L Zhang, M Xing, Z Bao, Velocity ambiguity resolving for moving target indication by compressed sensing. Electron. Lett. **47**, 1249–1251 (2011)
26. D Model, M Zibulevsky, Signal reconstruction in sensor arrays using sparse representations. Signal Process. **86**(3), 624–638 (2006)
27. L Carin, L Dehong, G Bin, Coherence, compressive sensing, and random sensor arrays. IEEE Antennas Propag. Mag. **53**(4), 28–39 (2011)
28. DL Donoho, Compressed sensing. IEEE Trans. Information Theory. **52**(4), 1289–1306 (2006)
29. H Nan, Y Zhongfu, X Xu, B Ming, Doa estimation for sparse array via sparse signal reconstruction. IEEE Trans. Aerospace Electron. Syst. **49**(2), 760–773 (2013)
30. W Jian, S Wei-Xing, H Yu-Bing, M Xiao-Feng, Adaptive beamforming with compressed sensing for sparse receiving array. IEEE Trans. Aerospace Electronic Syst. **50**(2), 823–833 (2014)
31. WJ Zhang Yin, J Yang, A sparse sampling strategy for angular superresolution of real beam scanning radar. EURASIP J. Adv. Signal Process. **2014**(1), 1–8 (2014)
32. DH Johnson, DE Dudgeon, *Array Signal Processing: Concepts and Techniques*. (Prentice-Hall, Englewood Cliffs, NJ, 1993)
33. MF Duarte, RG Baraniuk, Kronecker compressive sensing. IEEE Trans. Image Process. **21**(2), 494–504 (2012)
34. AW PR Gill, A Molnar, The in-crowd algorithm for fast basis pursuit denoising. IEEE Trans. Signal Process. **59**, 4595–4605 (2011)
35. JA Tropp, Just relax: convex programming methods for identifying sparse signals in noise. IEEE Trans. Inform. Theory. **52**, 1030–1051 (2006)
36. M Elad, Optimized projections for compressed sensing. IEEE Trans. Signal Process. **55**(12), 5695–5702 (2007)
37. J Xu, Y Pi, Z Cao, Optimized projection matrix for compressive sensing. EURASIP J. Adv. Signal Process. **43**, 1–8 (2010)
38. L Gang, Z Zhihui, Y Dehui, C Liping, B Huang, On projection matrix optimization for compressive sensing systems. IEEE Trans. Signal Process. **61**(11), 2887–2898 (2013)
39. JM Duarte-Carvajalino, G Sapiro, Learning to sense sparse signals: simultaneous sensing matrix and sparsifying dictionary optimization. IEEE Trans. Image Process. **18**(7), 1395–1408 (2009)
40. MF Duarte, MA Davenport, D Takhar, JN Laska, S Ting, KF Kelly, RG Baraniuk, Single-pixel imaging via compressive sampling. IEEE Signal Process. Mag. **25**(2), 83–91 (2008)
41. EJ Candes, J Romberg, T Tao, Robust uncertainty principles: exact signal reconstruction from highly incomplete frequency information. IEEE Trans. Inform. Theory. **52**(2), 489–509 (2006)
42. D Karaboga, B Basturk, A powerful and efficient algorithm for numerical function optimization: artificial bee colony (abc) algorithm. J. Global Optimization. **39**(3), 459–471 (2007)
43. DLD SS Chen, MA Saunders, Atomic decomposition by basis pursuit. SIAM J. Sci. Comput. **43**, 129–159 (2001)
44. J Zhang, W Wu, D-G Fang, Comparison of correction techniques and analysis of errors for digital beamforming antenna array with single rf receiver. IEEE Trans. Antennas Propag. **60**(11), 5157–5163 (2012)